Method of Moments Solution for the Characteristics of a Disk-Loaded Cylindrical Dipole Antenna

Won-Seo Cho*, Kyu-Don Choi**, Jung-Ki Kim***, and Ho-Jung Hwang***
Regular Members

ABSTRACT

The characteristics of a disk-loaded cylindrical dipole (DLCD) antenna that determine its performance are analyzed by using the method of moments. The current integral equation that is considered with extended boundary condition is derived. Numerical results for the input impedance and radiation pattern of the antenna are presented. The antenna factor with the antenna gain is computed to check the possibility of using this antenna as the broadband antenna for the special case in such as electromagnetic compatibility testing. The comparisons of the computed results with measured data are made. These results will allow this antenna to be used with confidence in various applications.

I. INTRODUCTION

Recently, there have been increasing demands for low profile antennas and their broadband operation to fulfill a variety of specifications[1]-[3]. In general, the need for these antennas arises because there is insufficient space to fit a conventional one and broadband measurements are required in such as electromagnetic compatibility (EMC) testing. Loading of electrically small dipole and monopole antennas to improve their input impedance characteristics for these requirements has been employed. Such techniques may use end-disks[4]-[6] or dielectric coating[7]. The DLCD antenna is shown in Fig. 1. This composite design can be chosen to obtain a low profile antenna of relatively broadband[1]. Such an antenna structure, however, is difficult to analyze because it includes some discontinuous surfaces. The diakoptic theory of multielement antennas of complex configuration, suggested Goubau et al.[3], takes a new approach to this problem. But the

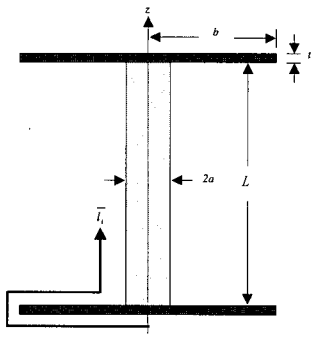

Fig. 1 Geometry of the disk-loaded cylindrical dipole (DLCD) antenna.

the theory involves hypothetical current sources which violate the current continuity condition. The modified theory, which allows an impedance matrix formulation to establish the relationship with the method of moments (MoM), was presented in[8]. The concept of cylindrical harmonic field expansions was developed for the analysis of an electrically short monopole with a circular top-hat[9],[10]. In this paper, we derive

* 산업기술시험원 전자파팀 (wscho@ktl.re.kr)
** 현대전자 정보통신연구소
*** 중앙대학교 전기전자공학부
논문번호 : 99178-0506, 접수일자 : 1999년 5월 6일

the current integral equation from Maxwell's equations that are applied to the whole structure of the DLCD antenna. The integral equation is obtained with using the extended boundary condition proposed by Waterman[11], who suggests that field relationships be imposed within a conducting body, rather than on its surface. In so doing no logarithmic singularity in a kernel of the integral equation is expected. For solving this equation the MoM is used along with the point-matching method. Representative numeri- cal results of the antenna are presented and some experimental data are also presented to support the numerical computation.

Ⅱ. INTEGRAL EQUATION

Cylindrical coordinates (ρ, ϕ, z) are oriented so that the vertical z-axis in Fig. 1 is centered through the antenna structure. Antenna length is given by L, while radii of the vertical stem and end disk having t thickness are respectively a and b. The integral equation for the surface current can be written by equating the total electric field inside a conductor to zero[11],[12], i.e.,

$$\bar{E}_t\big|_{inside} = \bar{E}^i + \bar{E}^s$$

$$= j\omega\varepsilon_0 \bar{E}^i + k^2 \int_{S'} \bar{J}(s')GdS' + \int_{S'} \bar{\nabla}' \cdot \bar{J}(s')\nabla GdS' = 0 \tag{1}$$

where the subscript t represents the total electric field and the superscripts i, s, and stand for the incident field, scatter field, and source points.

In the geometry of Fig. 1 the surface current flows in the z and ϕ directions of the cylindrical dipole element and in the ρ and ϕ directions of the end disks respectively. In this case, the current of the ϕ direction component for whole antenna structure can be neglected since the symmetrical geometry and ideal feeding for this antenna can be established. For simplicity of integration the antenna is subdivided into seven sections (l_i, $i=1,2,3,...7$). The current density J (s) is not a function of the azimuthal angle ϕ' but a function of ρ' or z' depending on each section of the antenna, and it can be expressed as

$$\bar{J}(s') = \frac{\bar{I}(l')}{2\pi\rho'} \tag{2}$$

where $I(l')$ is assumed to be an equivalent filament current located at radial distance $\rho'=a$ in l_4 and $\rho'=b$ in l_2 and l_6, and also at distance $0 \le \rho' \le b$ in l_1 and l_7, and $a \le \rho' \le b$ in l_3 and l_5. Thus we can rewrite the integral equation of (1) as

$$\int_{l'} \bar{\nabla}' \cdot \frac{\bar{I}(l')}{\rho'} \int_0^{2\pi} \frac{1}{2\pi} \left(\frac{\partial}{\partial\rho} G\bar{a}_\rho + \frac{\partial}{\partial z} G\bar{a}_z \right) \rho' d\phi' dl'$$

$$+ k^2 \int_{l'} \bar{I}(l') \int_0^{2\pi} \frac{G}{2\pi} d\phi' dl' = -j\omega\varepsilon_0 \bar{E}^i \tag{3}$$

where

$$G = \frac{e^{-jkR}}{4\pi R} \tag{4}$$

$$R = \sqrt{\rho^2 + \rho'^2 - 2\rho\rho'\cos(\phi') + (z-z')^2}\,. \tag{5}$$

When we apply into (3) the condition that the current at the center of the outside of the end disks is zero and the observation points are located inside the antenna structure, we obtain the final integral equation as

$$\bar{a}_o \cdot \left\{ \sum_i^{1,3,5,7} \int_{\rho_i'} I(\rho') \left[\left(k^2 - \frac{\partial^2}{\partial\rho'\partial\rho} \right) \bar{a}_\rho - \frac{\partial^2}{\partial\rho'\partial z} \bar{a}_z \right] G^* d\rho' \Big|_{z'=c} \right.$$

$$\left. + \sum_i^{2,4,6} \int_{z_i'} I(z') \left[-\frac{\partial^2}{\partial z'\partial\rho} \bar{a}_\rho + \left(k^2 - \frac{\partial^2}{\partial z'\partial z} \right) \bar{a}_z \right] G^* dz' \Big|_{\rho'=c} \right\}$$

$$= -j\omega\varepsilon_0 \bar{a}_o \cdot \bar{E}^i \tag{6}$$

where

$$G^* = \int_0^{2\pi} \frac{G}{2\pi} d\phi' \tag{7}$$

and $\bar{a}_o$ represents the vector on the observation

inside the antenna and c means constant value. In order to solve (6) for the antenna current $I(\rho', z')$, the MoM is used. Accordingly, the antenna is divided into N segments. The unknown current $I(\rho', z')$ is expanded in a set of N pulse basis functions as

$$I(\rho', z') = \sum_{n=1}^{N} I_n P_n(\rho', z') \tag{8}$$

where I_n are constants to be determined. Substitution of the current expansion (8) into (6) with the moment procedure[13] yields an $N \times N$ system of linear equations, which may be written in a matrix form as

$$[Z_{mn}][I_n] = [E_m] \tag{9}$$

where$[Z_{mn}]$ is the $N \times N$ moment matrix and$[I_n]$ and$[E_m]$ are the current coefficient column vector and the incident field column vector of length N. The impedance matrix and impressed field matrix elements are given by

$$Z_{mn} = \begin{cases} \int_{p_n-\Delta/2}^{p_n+\Delta/2} \left(k^2 - \dfrac{\partial^2}{\partial \rho' \partial \rho} \right) G^* d\rho' & (\rho_i' \text{ and } \bar{a}_o : \rho \text{ direction}) \\ \int_{p_n-\Delta/2}^{p_n+\Delta/2} \left(-\dfrac{\partial^2}{\partial \rho' \partial z} \right) G^* d\rho' & (\rho_i' \text{ and } \bar{a}_o : z \text{ direction}) \\ \int_{p_n-\Delta/2}^{p_n+\Delta/2} \left(-\dfrac{\partial^2}{\partial z' \partial z} \right) G^* dz' & (z_i' \text{ and } \bar{a}_o : z \text{ direction}) \\ \int_{p_n-\Delta/2}^{p_n+\Delta/2} \left(k^2 - \dfrac{\partial^2}{\partial z' \partial \rho} \right) G^* d\rho' & (z_i' \text{ and } \bar{a}_o : \rho \text{ direction}) \end{cases} \tag{10}$$

$$E_m = \begin{cases} -j\omega\varepsilon_0 E_\rho(\rho_m, z_m), & (\bar{a}_o : \rho \text{ direction}) \\ -j\omega\varepsilon_0 E_z(\rho_m, z_m), & (\bar{a}_o : z \text{ direction}) \end{cases} \tag{11}$$

where

$$G^* = \begin{cases} \int_0^{2\pi} \dfrac{e^{-jk\sqrt{\rho_m^2 + \rho'^2 - 2\rho_m\rho'\cos(\phi') + (z_m - z_n)^2}}}{8\pi^2\sqrt{\rho_m^2 + \rho'^2 - 2\rho_m\rho'\cos(\phi') + (z_m - z_n)^2}} d\phi' \\ (p_n : \rho' \text{ component}) \\ \int_0^{2\pi} \dfrac{e^{-jk\sqrt{\rho_m^2 + \rho_n^2 - 2\rho_m\rho_n\cos(\phi') + (z_m - z')^2}}}{8\pi^2\sqrt{\rho_m^2 + \rho_n^2 - 2\rho_m\rho_n\cos(\phi') + (z_m - z')^2}} d\phi' \\ (z_n : z' \text{ component}) \end{cases} \tag{12}$$

The problem for the current distribution of the DLCD antenna has been formulated in this section. Once the elements of the moment matrix and the impressed field matrix are determined, the unknown coefficients can be found by solving the resulting system of linear equation (9) with matrix inversion technique. In this paper the solution described uses pulse subsection currents and point-matching method, while the antenna is assumed to be excited by an idealized source, the magnetic frill generator.

Ⅲ. RESULTS AND DISCUSSION

A. Input Impedance

The input impedance of the antenna is obtained from the ratio of an input excitation and the current at the input terminal of the antenna. The DLCD antenna considered has the dimensions of L=500mm, a=19mm, b=87mm, and t=5mm. Fig. 2 illustrates the computed variation of the input impedance of the DLCD antenna and that antenna without disk between 20 MHz and 1000 MHz. It can be seen from the figure that the input resistance decreases while the capacitive reactance increases rapidly below about 200 MHz for the antenna and below about 300 MHz for the antenna without disk. Matching this varying impedance to a 50 Ω cable is not a trivial task. Usually, a balun transformer with an appropriate turn ratio is used such that some mean value of antenna impedance is chosen, which minimizes the reflection coefficient at the junction between antenna and cable. The computed resonant frequency of the antenna is 160 MHz whereas that of the antenna without disk is 250 MHz. It implies that loading the disk moves the resonant frequency of the antenna. The variation of the voltage standing wave ratio (VSWR) for different disk radii, b is shown in Fig. 3. It is clear from the graph that as the radius of disk increases the resonant frequency decreases and the bandwidth decreases. However, the resonant frequency does not decrease any more from a specific point although the radius increases. In case of Fig. 3

the specific point is b=8.5a. It also implies that combination of the radius of disk and the length of dipole element can decide the frequency range of interest.

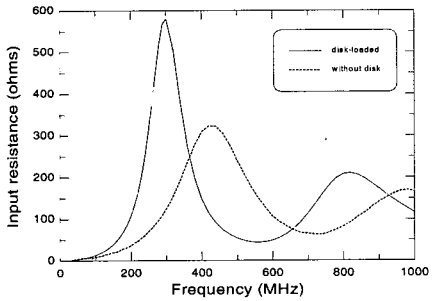

(a)

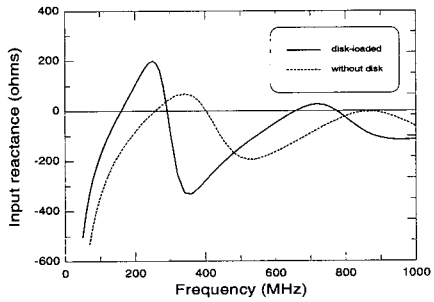

(b)

Fig. 2 Input impedance comparison between the DLCD antenna and that antenna without disk.
(a) Input resistance.
(b) Input reactance.
L=500mm, a=19mm, b=87mm, and t =5mm.

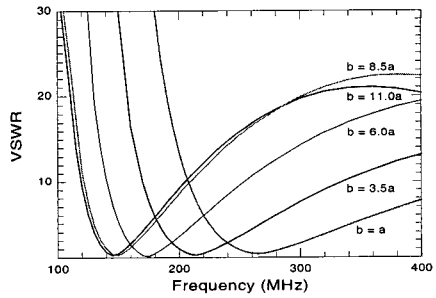

Fig. 3 Comparison of the VSWR for different disk radii, b. L=500mm, a=10mm, and t =5mm.

B. Radiation Pattern

In order to compute the radiation pattern, the current distribution derived from (9) with Maxwell's equation is used[14]. The far-zone electric field components for the antenna can be expressed as

$$E_\theta = -jk\eta_0 \frac{e^{-jkr}}{4\pi r}(C_\rho(\theta)\cos\theta - C_z(\theta)\sin\theta) \tag{13}$$

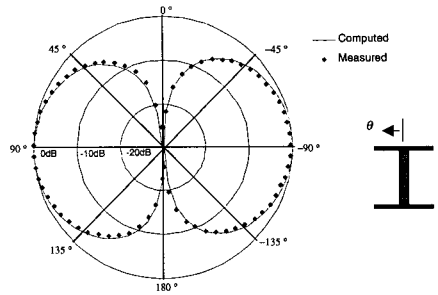

Fig. 4 Computed and measured results of the normalized radiation pattern at 160 MHz.
L=500mm, a=19mm, b=87mm, and t =5mm.

where

$$C_\rho(\theta) = \sum_i^{1,3,5,7} \int_{\rho_i'} I(\rho') e^{jk(z_n' \cos\theta + \rho' \sin\theta)} d\rho' \tag{14}$$

$$C_z(\theta) = \sum_i^{2,4,6} \int_{z_i'} I(z') e^{jk(z' \cos\theta + \rho_n' \sin\theta)} dz' . \tag{15}$$

Fig. 4 shows the computed and measured results for the radiation pattern at 160 MHz. It can be seen from the plots that the agreement between the results is quite good. The agreement would therefore seem to confirm the validity of the analysis in this paper. For emission testing, and radio monitoring site survey, the antenna should be omnidirectional[15]. The DLCD antenna has the pattern available to such an application. The radiation plot is very similar to that of the resonant dipole antenna.

C. Antenna Factor

Measurements of radiated emissions from the equipment under test are usually made in the frequency range from 30 MHz to 1000 MHz. Both the CISPR-16[16] and ANSI C63.2[17] regulations on EMC measurements allow suitable broadband antennas to be instead of resonant dipole antennas, as long as they satisfy certain beamwidth, VSWR, and polarization criteria. Before any antenna can be used for radiated emission measurements, it is necessary that its antenna factor (AF) be known accurately over the

frequency range of interest. In this paper with considering AF, we investigate the DLCD antenna for EMC measurements. The AF of receiving antenna from[18] is defined as

$$AF = \frac{2}{\lambda}\sqrt{\frac{\pi\eta_0}{G_r(\theta,\phi)R_r M}} \tag{16}$$

where M indicates the impedance mismatch loss between the antenna and the measuring receiver with input impedance R_r, $G_r(\theta,\phi)$ is the power gain of the antenna as a function of the angle of arrival of the energy, $\eta_0 = 120\,\Omega$ is the intrinsic impedance of free space, and λ is the wavelength. Fig. 5 shows the computed and measured AF with the gain and the mismatch loss in the frequency range from 30 MHz to 500 MHz. The gain $G_r(\theta,\phi)$ is computed at $\theta = 90°$ and $\phi = 0°$. It is evident that the AF and the mismatch loss are the lowest values at the resonant frequency. Below about 150MHz, the AF increases while the mismatch loss increases. It implies that the AF below the resonant frequency is mainly related with the mismatch loss. AF measurement with the reference antenna method specified in ANSI C63.5[19] was performed at the 10m site of Korea Testing Laboratory. The reference antenna method provides a method of antenna calibration based on the use of a dipole with a well-matched balun whose construction is described in that standard. The measured and computed results are in good agreement.

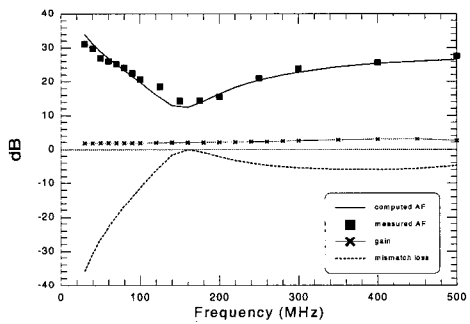

Fig. 5 Variation with frequency of the computed antenna factor, antenna gain and mismatch loss as well as the measured antenna factor of the DLCD antenna. L=500mm, a=19mm, b=87mm, and t=5mm.

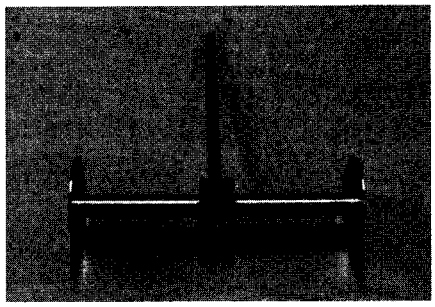

Fig. 6 Photograph of the DLCD antenna designed for experimental results.

Ⅳ. CONCLUSION

The characteristics and performance of the DLCD antenna have been described in this paper. The input impedance, and radiation pattern as well as the gain of the antenna were obtained by using the MoM. Also, the AF was computed and measured for the special case where the antenna is used for EMC testing. The results show the possibility of using this antenna as the broadband antenna with improved AF in EMC measurements. Since the computed and measured values for all of the results are in good agreement, the validity of the analysis in this paper is confirmed. The aim of future work is to design DLCD antennas for EMC testing and site validation[16] with the characteristics of improved AF and bandwidth. The antenna designed for experimental results is shown in Fig. 6.

REFERENCE

[1] K. Fujimoto, A. Henderson, K. Hirasawa and J. R.James, *Small Antennas*, Research Studies Press Ltd., pp. 1-29, 1987.

[2] Goubau, Multi-element monopole antennas, in *Proc. ECOM-ARO Workshop on Electrically Small Antennas*, Forth Monmouth, NJ, pp. 63-67, Oct. 1976.

[3] G. Goubau, N. N Puri and F. K Schwering, Diakoptic Theory for Multielement Antennas, *IEEE Trans. Antennas and Propagat.*, vol.

AP-30, no. 1, pp. 15-26, 1982.

[4] A. F. Gangi, S. Sensiper, and G. R. Dunn, The characteristics of electrically short umbrella top-loaded antennas, *IEEE Trans. Antennas and Propagat.*, vol. AP-13, no. 6, pp. 864-871, 1965.

[5] Won-Seo Cho, Kyu-Don Choi and Jung-Ki Kim, Characteristics of a Cylindrical Dipole Antenna with End Disks, *in Proc. 8th CEFC IEEE Magnetics,* Arizona, pp.166, 1998.

[6] Won-Seo Cho, Kyu-Don Choi and Jung-Ki Kim, Analysis of a Thick Dipole Antenna with End Disks, *in Proc. Intern. Symp. on EMC,* Roma, pp.747-751, 1998.

[7] C. Y. Ying, Theoretical study of finite dielectric-coated cylindrical antennas, *J. Math Physics,* vol. 10, pp. 480-483, 1969.

[8] F. K Schwering, N. N Puri and C. M. Butler, Modified Diakoptic Theory of Antennas, *IEEE Trans. Antennas and Propagat.,* vol. AP-34, no. 11, pp. 1273-1281, 1986.

[9] F. K Schwering, N. N Puri and A. Stavridis, The Modal Expansion solution of a Top Loaded Monopole, *in Abstracts for the 1982 IEEE AP-S Symposium,* Albuquerque, NM., pp. 584-587.

[10] M.A. Morgan and F. K Schwering, Eigenmode Analysis of Dielectric Loaded Top-Hat Monopole Antennas, *IEEE Trans. Antennas and Propagat.,* vol. AP-42, no. 1, pp. 54-61, 1994.

[11] P. C. Waterman, New formulation of acoustic scattering, *J. Acost. Soc. Amer.,*vol. 45, pp. 1067-1429, June 1969.

[12] C. D. Taylor and D. R. Wilton, The Extended Boundary Condition Solution of the Dipole Antenna of Revolution, *IEEE Trans. Antennas and Propagat.,* vol. AP-20, no. 6, pp. 772-776, Nov. 1972.

[13] R. F. Harrington, *Field Computation by Moment Methods.* New York : Macmillan, pp. 1-21, 1968.

[14] Balanis, *Antenna Theory : analysis and design,* 2nd ed. New York : John Wiley & Sons Inc., pp. 133-159, 1997.

[15] T. Macnamara, *Handbook of Antennas for EMC,* Norwood : Artech House Inc., pp. 1-33, 1995.

[16] CISPR-16, Specification for radio Interference Measuring Apparatus and Measurement Methods (2nd. ed.), 1987.

[17] ANSI C63.2, Specifications for Electromagnetic Noise and Field Strength Instrumentation, 10kHz to 1GHz, 1980.

[18] B. A. Austin and A. P. C. Fourie, Characteristics of the Wire Biconical Antenna Used for EMC Measurements, *IEEE Trans. Electromagn. Compat.,* vol. EMC-33, no. 3, pp. 179-187, Aug. 1991.

[19] ANSI C63.5, Calibration of Antennas Used for Radiated Emission Measurements in Electromagnetic Interference (EMI) Control, 1998.

조 원 서 (Won-Seo Cho) 정회원

1997년~현재 중앙대학교 박사수료

1991년~현재 산업기술시험원 선임 연구원

<주관심 분야> EMC 및 전자파 표 준개발, EMC 안테나 해석 및 교 정기술, 전자파 흡수 및 차폐 측 정기술 개발

최 규 돈 (Kyu-Don Choi) 정회원

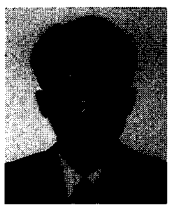

1998년 중앙대학교 (공학석사)

1998년~현재 현대전자 정보통신 연구소 연구원

<주관심 분야> IMT-2000, 위성통신 기술, Microwave 및 안테나 관련 기술개발

김 정 기 (Jung-Ki Kim) 정회원

1977년~1998년 중앙대학교 교수

한국통신학회논문지 제24권 10호 참조

황 호 정 (Kyu-Don Choi) 정회원

1982년 Tech. University of Munich, Germany (공학박사)
1983~현재 중앙대학교 전기전자 제어공학부 교수

<주관심 분야> 반도체공정 시뮬레 이션, 반도체 기술 및 측정